Rate constant of the reaction between CH3O2 and OH radicals

Adriana Bossolasco, Eszter Pongráczné Faragó, Coralie Schoemaecker, Christa Fittschen

Rate Constant of the Reaction between CH_3O_2 and OH Radicals

Adriana Bossolasco[1,2], Eszter P. Faragó[1,3], Coralie Schoemaecker[1], Christa Fittschen[1,*]

[1]*PhysicoChimie des Processus de Combustion et de l'Atmosphère PC2A, CNRS - University Lille 1, Cité Scientifique, Bât. C11, 59655 Villeneuve d'Ascq, France*

[2]*INFIQC (CONICET), Departamento de Fisicoquímica, Facultad de Ciencias Químicas, Universidad Nacional de Córdoba, Córdoba, Argentina*

[3] *Department of Chemical Informatics, Faculty of Education, University of Szeged, Szeged, Boldogasszony sgt. 6. Hungary 6725*

*Corresponding author: Christa Fittschen (christa.fittschen@univ-lille1.fr)

Re-revised version

Submitted to

Chemical Physics Letters

Abstract

The rate constant of the reaction

$$OH + CH_3O_2 \rightarrow \text{products} \qquad \text{(R1)}.$$

has been measured at 294K by simultaneous coupling of Laser Induced Fluorescence (LIF) and cw-Cavity Ring Down Spectroscopy (cw-CDRS) to laser photolysis. OH radicals were generated by 248nm photolysis of either O_3 in the presence of H_2O or H_2O_2, CH_3O_2 radicals were generated simultaneously by photolysis of CH_3I and their absolute concentrations were obtained by cw-CRDS. OH decays were measured under excess CH_3O_2 concentrations and a very fast rate constant of $k_1 = (2.8\pm1.4)\times10^{-10}cm^3s^{-1}$ was found independent of pressure at 50 and 100 Torr helium.

Introduction

Peroxy alkyl radicals (RO_2) are key reaction intermediates in the low temperature oxidation of organic compounds and play a central role in atmospheric chemistry [1]. They are predominantly formed from the initial reaction of OH radicals with hydrocarbons, leading to formation of an alkyl radical R:

$$RH + OH \rightarrow R + H_2O \qquad (R2)$$

followed by recombination of the alkyl radical with molecular oxygen

$$R + O_2 \rightarrow RO_2 \qquad (R3)$$

In polluted environments, peroxy radicals react predominantly with NO, leading to formation of NO_2, which through subsequent photolysis leads to formation of O_3.

At low NOx concentrations such as in the remote continental boundary layer, the marine boundary layer, and the background troposphere, the lifetimes of RO_2 radicals increase and other reaction pathways become competitive for peroxy radicals. Atmospheric chemistry models consider the major fate for RO_2 radicals under these conditions through self- and cross reactions with other RO_2 radicals or with HO_2 radicals [2], in the example of CH_3O_2:

$$CH_3O_2 + CH_3O_2 \rightarrow 2\ CH_3O + O_2 \qquad (R4a)$$

$$\rightarrow\ CH_2O + CH_3OH + O_2 \qquad (R4b)$$

$$CH_3O_2 + HO_2 \rightarrow CH_3O_2H + O_2 \qquad (R5)$$

Currently, the reaction of RO_2 radicals with OH radicals is not considered in models, even though if fast enough to compensate for the roughly 2 orders of magnitude lower OH concentration compared to HO_2 or RO_2, it might become competitive with (R4) and (R5). In a recent modeling study, Archibald and co-workers [3] have investigated the impact of including the reaction between RO_2 and OH on the composition of the Marine Boundary Layer (MBL). They have run different scenarios using a model named BAMBO, based on the MCM mechanism [2]. Different possible reaction paths and rate constants were simulated for peroxy radicals up to C4, leading for the simplest one, CH_3O_2, to the following products:

$$OH + CH_3O_2 \rightarrow CH_2O_2 + H_2O \qquad (R1a)$$

$$OH + CH_3O_2 \rightarrow CH_3O + HO_2 \qquad (R1b)$$

$$OH + CH_3O_2 \rightarrow CH_3OH + O_2 \qquad (R1c)$$

For all scenarios they found only a small, negligible effect on the mixing ratios of O_3, NO_x, OH and other trace gas species in the marine boundary layer. However, a substantial increase in the mixing ratios of HCOOH was observed (from 0.16 ppt in the base case, i.e. absence of

(R1), to 25.5 ppt at the highest rate constant scenario), if the reaction pathway would be formation of the Criegee radical (R1a). A strong increase in the mixing ratio of CH_3OH (from 37 ppt in the base case, i.e. absence of (R1), to 294 ppt at the highest rate constant scenario), was observed if the major pathway would be (R1c). The impact on the RO_2 and HO_2 radical budget was below 10% for all scenarios.

Besides a direct interest in the rate constant of the title reaction through its possible impact onto the atmospheric composition, there is also a fundamental interest: radical-radical reactions are difficult to measure and to our knowledge, the reaction between OH radicals and alkyl-peroxy radicals has never been studied experimentally. The only estimation of the rate constant of the title reaction has been carried out by Tsang and Hampson [4]: based on analogy with the reaction of HO_2 with OH radicals, they recommended for the reaction between CH_3O_2 and OH a rate constant of k_1 = 1.0 x 10^{-10} cm^3s^{-1} with an estimated uncertainty of a factor of 5. In the absence of any experimental study of the title reaction, the reaction of CH_3O_2 radicals with Cl-atoms can serve as proxy: it has been investigated several times [5,[6,[7,[8] and its rate constant is very fast (≈ 1.7×10^{-10} cm^3s^{-1}), proposed reaction products are either CH_3O and CH_2O_2 (corresponding to (R1a) and (R1b)) in equal amounts [5,[6] while Daële and Poulet [8] suggest (R1a) as the major channel. Biggs *et al*. [9] have investigated experimentally the reaction of the most simple fluorinated peroxy radical CF_3O_2 with OH. They determined a rate constant for this reaction of (4.0 ± 0.3) x10^{-11} cm^3s^{-1} at 296 ± 1 K with the product probably being HO_2 radicals. The same reaction has also been investigated theoretically by Du and Zhang [10]: DFT calculations have shown a multitude of possible reaction products, with CF_3O + HO_2 being the major products on the triplet surface, while the situation is more complicated on the singlet surface.

Taking into account the total lack of any experimental or theoretical study of alkyl-peroxy radicals with OH radicals and their potential impact in low NOx environments, we have investigated the reaction of the most simple alkyl-peroxy radical, CH_3O_2, with OH.

Experimental Setup

The experimental setup has been described in detail in earlier papers [11,[12], a recent improvement on the continuous wave Cavity Ring Down Spectrometer (cw-CRDS) system has been described by Votava *et al.* [13]. Briefly, the setup consists of the photolysis cell, the photolysis laser (Lambda Physic LPX 202i), the cw-CRDS system, and the high repetition rate (10 kHz) Laser Induced Fluorescence (LIF) system [14].

CH_3O_2 radicals were generated by the 248 nm photolysis of CH_3I in the presence of O_2:

$$CH_3I + h\nu_{248nm} \rightarrow CH_3 + I \qquad \text{(R6)}$$

$$CH_3 + O_2\,(+M) \rightarrow CH_3O_2\,(+M) \qquad \text{(R7)}$$

Absolute time-resolved CH_3O_2 concentration profiles have been measured at one of the most intense absorption peaks of the ν_{12} - transition of the A←X band at 7489.16 cm^{-1} using the absorption cross section such as obtained in a recent work in our laboratory ($\sigma = 3.40 \times 10^{-20}$ cm^2 independent of pressure) [15]. Ring-down times were converted to CH_3O_2 concentrations using the following equation:

$$[CH_3O_2] = \frac{R_L}{c \times \sigma}\left(\frac{1}{\tau} - \frac{1}{\tau_0}\right) \qquad \text{[Eq. 1]}$$

where R_L is the ratio between the cavity length L, i.e., the distance between the two cavity mirrors (82 cm), and the length L_A over which the absorber is present (in our case the overlap of photolysis beam and absorption path, 28.7 cm), c is the speed of light. Finally, τ_0 and τ are the ring-down times in the absence (before the photolysis pulse) and in the presence (after the photolysis pulse) of CH_3O_2, respectively.

OH radicals were co-generated by the simultaneous photolysis of an appropriate precursor: in most experiments, O_3 has been photolysed in the presence of H_2O:

$$O_3 + h\nu_{248nm} \rightarrow O(^1D) + O_2 \qquad \text{(R8)}$$

$$O(^1D) + H_2O \rightarrow 2\ OH \qquad \text{(R9a)}$$

whereby O_3 is generated continuously by a commercial ozone generator (UVP-SOG 2) through photolysis of O_2 by a mercury lamp, leading to $O(^3P)$ atoms, which in turn recombine with O_2 leading to O_3. The major fraction of $O(^1D)$, generated within the photolysis reactor, will be quenched by collision mostly with O_2, leading to $O(^3P)$:

$$O(^1D) + M \rightarrow O(^3P) + M \qquad \text{(R9b)}$$

The possible influence of these $O(^3P)$ on the OH-decays will be discussed further down. In a few complementary experiments, H_2O_2 photolysis at 248 nm, known as a clean OH-source [16,[17], has been used as a precursor, thus excluding possible complications due to $O(^3P)$ chemistry. Relative time-resolved OH radical concentration profiles were detected by high repetition rate LIF (10 kHz) [14]. OH is excited in the (1-0) vibrational band of the A-X electronic transition at around 282 nm and the fluorescence is collected perpendicular to the laser beams through an interference filter at 310 ± 20 nm with a photomultiplier and a Boxcar integrator (EG&G Model 412B).

All experiments were carried out at 294 K and at two different total pressures, 50 and 100 Torr. Total gas flows were 306 and 640 cm^3min^{-1} at 50 and 100 Torr, respectively. Such flows assured a renewal of the gas mixture between two photolysis laser shots (repetition rate being 0.2 Hz). The different gases were introduced into the reactor as stabilized flows using calibrated flow controllers (Bronkhorst and Tylan) and the total pressure was kept constant using a pressure controller (Leybold-Heraeus MR16) installed at the exit of the reactor. Helium (Praxair, 6.0) and O_2 (Praxair, 4.5) were used without further purification, H_2O was admitted to the cell by bubbling a fraction of the main helium flow through a bubbler filled with ultrapure H_2O, CH_3I (Aldrich, 99%) was prepared as a 1% mixture in helium in darkened glass bulbs. At 50 / 100 Torr total pressure, the concentrations were: $[O_2] = 5.1 / 2.8 \times 10^{17}$ cm^{-3}, $[H_2O] = 2.5 / 7.6 \times 10^{15}$ cm^{-3} and $[CH_3I]$ has been varied for both pressures between $(2.4 – 6) \times 10^{14}$ cm^{-3}. The laser energy was varied between 13 and 22 mJ cm^{-2}, leading to initial CH_3O_2 concentrations between 3 and 13×10^{12} cm^{-3}. Some experiments have been carried out to verify the concordance of the employed absorption cross section of CH_3O_2 with the results from our earlier measurements, carried out at higher CH_3O_2 concentrations [15]: for these experiments, CH_3O_2 concentrations of up to 40×10^{12} cm^{-3} have been used.

For experiments with H_2O_2 as precursor, it was introduced into the reactor by bubbling a fraction of the main helium flow through a 50% solution of H_2O_2 in H_2O. From the OH decay in absence of CH_3I, the H_2O_2 concentration was estimated to be 2.5×10^{13} cm^{-3}, leading to initial OH-concentrations of around 1×10^{11} cm^{-3}.

For O_3-experiemnts, a rough estimate of the initial O_3 and $O(^3P)$ concentration can be obtained from OH-decays in the absence of CH_3I (≈50 and 180 s^{-1} at 100 and 50 Torr, respectively). Under our typical photolysis energies (30 mJ cm^{-2}), around one third of the

initial O_3 will be photolysed. Under these conditions the major sink for OH-radicals becomes the reaction with $O(^3P)$

$$OH + O(^3P) \rightarrow O_2 + H \qquad (R10)$$

(k_{10} = 3.5×10^{-11} cm^3s^{-1}), together with minor contributions from the much slower reaction with O_3

$$OH + O_3 \rightarrow HO_2 + O_2 \qquad (R11)$$

(k_{11} = 7.3×10^{-14} cm^3s^{-1}) and diffusion out of the photolysis volume (≈5 and 15 s^{-1} at 100 and 50 Torr, respectively [18]). Therefore, an $O(^3P)$ concentration of around 1 / 5×10^{12} cm^{-3} can be estimated for the experiments at 100 / 50 Torr, respectively, leading to initial O_3 concentrations of around 3 / 15×10^{12} cm^{-3} at 100 / 50 Torr, respectively. Only a few percent of the initial $O(^1D)$ will be converted to OH radicals under our conditions (depending on H_2O and O_2 concentrations), leading to low OH-concentrations compared to CH_3O_2.

However, $O(^3P)$ has no impact on the OH decays in the presence of CH_3O_2 because (a) OH decays are much faster under these conditions and (b) $O(^3P)$ will react predominantly with CH_3I under these conditions:

$$CH_3I + O(^3P) \rightarrow CH_3 + IO \qquad (R12a)$$

$$\rightarrow OH + CH_2I \qquad (R12b)$$

$$\rightarrow \text{products} \qquad (R12c)$$

(R12) has been studied several times [19,[20,[21] and consistent rate constants between k_{12} = (1.7 and 2.0)$\times10^{-11}$ cm^3s^{-1} were found, leading to pseudo-first order rates that are fast on the time scale of our OH decays. The consequence of pathway (a) is, under our conditions, formation of additional CH_3O_2 radicals with a branching ratio of 0.44 [20], but also a rapid formation of IO. The possible role of IO in our reaction system will be discussed further down. Pathway (b) leads to a rise of the OH-concentration in the first 300 µs.

Result and discussion

CH_3 radicals are generated through the photolysis of CH_3I and are converted to CH_3O_2 radicals through reaction (R8) within a few 10 µs under our experimental conditions. The rate constant k_8 has been measured at low pressure (1-6 Torr helium and argon) by Selzer *et al.* [22], while the high pressure limit has been determined by Fernandes *et al.* [23]. From these values, k_8 under our conditions can be estimated to $k_8 = 1.4 / 2.1 \times 10^{-13}$ cm^3s^{-1}, i.e. $k_8' = 7.2 / 5.9 \times 10^4$ s^{-1} for 50 / 100 Torr He, respectively. As it turned out that the rate constant k_1 is extremely fast, low initial CH_3 concentrations were generated in these experiments such that the OH radicals decayed on a suitable time scale, *i.e.,* pseudo-first order decays on the order of a few 1000 s^{-1} ($[CH_3O_2]_{0,max} = 1.3\times10^{13}$ cm^{-3}, see below). Therefore, other radical-radical reactions that might change the initial composition of the gas mixture (such as $CH_3 + CH_3O_2$ or $CH_3 + CH_3$) are slow compared to (R8) and can be neglected: a model shows, that under our conditions the CH_3O_2 concentration reaches its maximum after 6 / 15 µs at 50 / 100 Torr and that around 96 / 92 % of the initial CH_3 radicals have been converted to CH_3O_2, the remaining 4 / 8 % being converted to C_2H_6 or CH_3O, whereby CH_3O will be converted to CH_2O and HO_2. The latter radical reacts fast with OH, however it has no impact on the OH decay mostly due to the delayed formation compared to the OH decays, but also due to their much lower concentration compared to CH_3O_2 radicals.

Figure 1 shows a typical example of simultaneously measured OH and CH_3O_2 traces. The time resolution of the OH-decay is 100 µs, corresponding to the repetition rate of the fluorescence excitation laser. OH-decays become exponential only after around 300 µs following the photolysis pulse, the initial rise is due to OH-formation in (R4b). The time resolution of the CH_3O_2 decay is random due to the synchronization mode of the experimental set-up [12]: raw data from individual ring down events are shown as open grey dots in **Figure 1**, while the red dots represent the average of ring-down events having occurred within a time-window of 1 ms. The insert shows the CH_3O_2 decay on a longer time scale (100 ms) and it can be seen that the CH_3O_2 concentration seems nearly stable on the time scale of the OH decay. However, using a simple extrapolation of the CH_3O_2 concentration to t = 0 s in order to extract the rate constant of the title reaction from the pseudo-first order decays of the OH profile bears the risk, that rapid side reactions alter the CH_3O_2 concentration at short times. On the other hand, the random time resolution makes it very tedious to obtain CH_3O_2 decays with a time resolution high enough to unravel details of its concentration-time profile on the

time scale of the OH-decays. Therefore, CH_3O_2 decays have been simulated by a model taking into account secondary chemistry with the goal of retrieving the CH_3O_2 concentration actually present during the short time window of the corresponding OH decay. The complete model used for simulating the concentration-time profiles is given in Table 1, and the rate constant of (R1) has been extracted in two steps: in a first step, the CH_3O_2 profile has been simulated on a time scale adapted to the CRDS measurements (up to 30 ms). The initial CH_3I and O_2 concentrations were obtained from pressure and flow meter readings, O_3 and $O(^3P)$ concentrations were estimated as explained above. Only the (identical) initial concentrations of CH_3 radicals and I-atoms were varied such that the experimental CH_3O_2 concentration was best reproduced over the first 30 ms. Once the initial radical concentrations were determined, the corresponding OH decay was simulated on a shorter time scale (2 – 5 ms, depending on the CH_3O_2 concentration): only the rate constant of the title reaction, k_1, was adjusted such that the corresponding experimental OH decay was best reproduced.

Possible side reactions that could alter the CH_3O_2 concentration on a short time scale are:

(a) self-reaction		(R4)
(b) with $O(^3P)$	$CH_3O_2 + O(^3P) \rightarrow CH_3O + O_2$	(R13)
(c) with I-atoms	$CH_3O_2 + I \rightarrow CH_3O_2I$	(R14)
	$CH_3O_2 I + I \rightarrow CH_3O_2 + I_2$	(R15)
(d) with IO radicals	$CH_3O_2 + IO \rightarrow$ products	(R16)

(a) The initial CH_3O_2 concentrations being very low, the self-reaction of the CH_3O_2 radicals with a recommended rate constant [24] of $k_4 = 3.5\times10^{-13}$ cm^3s^{-1} is also very slow and can be safely neglected on the time scale of the OH decays.

(b) The reaction of CH_3O_2 with $O(^3P)$-atoms has been studied by Zellner et al. [25] and a rate constant of $k_{13}=(4.3\pm2.0)\times10^{-11}$ cm^3s^{-1} has been found, which leads under our conditions to pseudo-first order decays of 120 – 400 s^{-1}, slow compared to the OH decays.

(c) The reaction of CH_3O_2 radicals with I-atoms has first been mentioned by Jenkin and Cox [26] and has more recently been studied in detail by Dillon et al. [27]. It was found that CH_3O_2 radicals catalyze the recombination of I-atoms in a Chaperon-like mechanism, with the rate constant for (R15) being roughly 10 times faster than for (R14). As a consequence, the CH_3O_2 concentration decreases rapidly by around 10% until the pseudo-first order rates of (R14) and (R15) are equalized. This decay occurs under our conditions within 1 to 2 ms, i.e., the time scale of our OH-decays, and therefore needs to be taken into account.

(d) Reaction (R16) has been studied several times: Enami et al. [28] as well as Bale et al. [29] report a rate constant of around 7×10^{-11} cm^3s^{-1}, while Dillon et al. [27,[30] have reported twice, using very different experimental set-ups and conditions, a rate constant 15 - 30 times slower (more discussion see further down).

In **Figure** 2 and 3 is shown the impact of (R13) to (R16) on the CH_3O_2 concentration-time profile. The upper panel of **Figure** 2 presents a CH_3O_2 profile for an experiment with a rather high initial radical concentration, the insert shows a zoom of the shaded area and represents the time scale of the OH decay, depicted on a logarithmic scale in the lower panel. The vertical dashed line indicates 300 µs, the time when the OH decays became exponential. Three different simulations of the mechanism in Table 1 are shown, which all reproduce very well the CH_3O_2 concentration at longer time scales. Differences however are visible in the zoom: (a) the lower, full line represents a model with the I and O(^{3}P) concentrations set to 0, ie., no secondary chemistry is taken into account; (b) the dashed line takes into account I-chemistry, ie., the I-atom concentration was set to the same value as the CH_3 concentration; (c) the dotted line finally represents the full model with additionally the O(^{3}P) concentration set to the estimated value. In order to reproduce CH_3O_2 at longer time scales, the initial CH_3 and I-concentrations need to be adjusted between the different simulations by 10-15 %. Fitting of the corresponding OH-decay leads to identical results for k_1 for (b) and (c), while neglecting any secondary chemistry would ask for an increase in the rate constant of the title reaction of around 10% in order to make up for the lower CH_3O_2 concentration: to illustrate the difference, all simulations in the lower panel use the same rate constant k_1, ie., the simulation (a) was not optimized for reproducing the OH decay.

Figure 3 shows the impact of IO chemistry (R16): a CH_3O_2 profile with low initial radical, but high O(^{3}P) concentration is depicted, conditions under which (R16) has the highest impact. The full model from Table 1 is run by using the two rate constants found in the literature: the full line represents the model with $k_{16} = 7\times10^{-11}$ cm^3s^{-1} such as proposed by Enami et al. [28] and Bale et al. [29], while the dashed line represents a model using $k_{16} = 3.4\times10^{-12}$ cm^3s^{-1}, the most recent value from Dillon et al. [30]. Again, the initial CH_3- and I-concentrations have been adjusted such that the CH_3O_2 concentration is best reproduced on longer time scales. It can be seen that under the conditions of this experiment the higher value for k_{16} leads to a strong decrease of the CH_3O_2 concentration on the time scale of typical OH-decays (few ms) and would therefore influence the retrieved value for k_1. However, such high rate constant for (R16) is not in agreement with the experimental CH_3O_2 profile. The lower

value for k_{17} influences the CH_3O_2 concentration only at long reaction times as can be seen from the slow rise of the product of (R16), represented by the grey lines. It has thus no impact on the retrieved value for k_1.

The rate constants such as obtained by fitting CH_3O_2 and OH decays to the full model, are summarized in **Table 2** and presented in **Figure 4** as a function of the initial radical concentration. No systematic trend is observed for the retrieved rate constant between the two different sets of experimental conditions (different pressure, $O(^3P)$ and O_3 concentration), which can be taken as another indication, that (R16)is too slow to influence the CH_3O_2 concentration profile on short time scales. The average value of the rate constant for (R1), obtained from fitting all experiments to the full model using the rate constants shown in Table 1, is $k_1 = (2.80 \pm 0.06) \times 10^{-10}$ cm^3s^{-1}, with the error being statistical only (95 % confidence interval), but other systematic errors need to be considered. Few experiments have been carried out using H_2O_2 as precursor, thus avoiding complications due to (R13 and (R16): a rate constant in excellent agreement with the one obtained using O_3 as an OH-precursor has been found.

However, with both precursors, the rate constant fully depends on the reliable determination of the CH_3O_2 concentration, any systematic error directly returns a proportional error in the rate constant k_1. The CH_3O_2 concentration has been obtained by applying [Eq. 1] to the time-resolved cw-CRDS measurements and thus transforming ring-down times into absolute CH_3O_2 concentrations. The absorption cross section (3.40×10^{-20} cm^2 at 7489.16 cm^{-1}) has recently been determined in our laboratory [15] in the same experimental set-up, using the same method for generating CH_3O_2 radicals. The absorption cross section was obtained from a kinetic analysis of the CH_3O_2 decay under conditions were self-reaction is preponderant, i.e. high concentrations. Indeed, considering the known rate constant of the self-reaction permits to retrieve the absolute initial CH_3O_2 concentration. This method has already been used earlier in our group [31] for the determination of the absorption cross sections of HO_2, which has later been confirmed using a different method by Tang *et al.* [32]. The cross section for CH_3O_2 determined in our group [15] is 2 to 3 times larger than earlier determinations by Pushkarsky *et al.* [33] and Atkinson and Spillman [34] using the same method, but plausible arguments have been presented by Farago *et al.* for this disagreement. A major source of uncertainty in the determination of the CH_3O_2 concentration is the uncertainty in the rate constant for the self reaction, on which is based the determination of the absorption cross section in all three experiments. An uncertainty of 30% is given by the IUPAC committee for

the rate constant k_1 [24], translating into the same uncertainty for the CH_3O_2 concentration. Another estimated uncertainty of 20% is added in order to take into account some dubiety remaining in the influence of secondary chemistry (R13) to (R16) on the CH_3O_2 concentration at short reaction times, leading to a final uncertainty of the rate constant of ± 50%:

$$k_1 = (2.8 \pm 1.4) \times 10^{-10}\ cm^3s^{-1}.$$

This very fast rate constant suggests that the impact of the reaction of peroxy radicals with OH radicals is not negligible under certain, remote condition and might be even more important than shown by Archibald *et al.*, who used rate constants of up to $1.5 \times 10^{-10}\ cm^3s^{-1}$ in his model. It should be noted however, that a lower absorption cross section for CH_3O_2 such as obtained by Pushkarsky *et al.* or Atkinson and Spillman would result in a lower rate constant: another determination of the absorption cross section of CH_3O_2 radicals would be most welcome. More laboratory studies are also needed to determine the rate constants of larger peroxy radicals with OH, and also, if possible, to determine the reaction products. High level *ab initio* calculations should be carried out in order to understand the mechanism of this very fast reaction and to determine the reaction pathway and product yields.

Conclusion

The rate constant of the reaction between the methylperoxy radical CH_3O_2, and the OH radical has been measured for the first time. Relative OH decays have been obtained by high repetition rate LIF in the presence of excess CH_3O_2. The absolute concentration of CH_3O_2 was measured simultaneously by time resolved cw-CRDS in the near IR. A very fast rate constant of $(2.8 \pm 1.4) \times 10^{-10}\ cm^3s^{-1}$, independent of pressure between 50 and 100 Torr, has been obtained. With such a fast rate constant, the reaction of CH_3O_2 radicals (and peroxy radicals in general) with OH radicals will be needed to be implemented into atmospheric chemistry models, as it will have non-negligible impact on the composition of the atmosphere especially in remote environments where NO_x concentrations are low and the lifetime of peroxy radicals is long.

Acknowledgement

The laboratory PC2A participates in the Institut de Recherche en ENvironnement Industriel (IRENI) which is financed by Région Nord Pas-de-Calais, the Ministère de l'Enseignement Supérieur et de la Recherche, the CNRS and European Regional Development Fund (ERDF). This project was supported by the French ANR agency under contract No. ANR-11-LabEx-0005-01 CaPPA (Chemical and Physical Properties of the Atmosphere). A.B. thanks the European Community for a scholarship within the frame of the EuroTango project. E.P.F acknowledges financial support from TÁMOP 4.2.2. A-11/1KONV-2012-0047. The authors thank the reviewers for helpful comments.

References

[1] G. S. Tyndall, R. A. Cox, C. Granier, R. Lesclaux, G. K. Moortgat, M. J. Pilling, A. R. Ravishankara, T. J. Wallington, J. Geophys. Res. 106 (2001) 12157-12182.

[2] S. M. Saunders, M. E. Jenkin, R. G. Derwent, M. J. Pilling, Atmos. Chem. Phys. 3 (2003) 161-180.

[3] A. T. Archibald, A. S. Petit, C. J. Percival, J. N. Harvey, D. E. Shallcross, Atmosph. Sci. Lett. 10 (2009) 102-108.

[4] W. Tsang, R. F. Hampson, J. Phys. Chem. Ref. Data 15 (1986) 1087.

[5] M. M. Maricq, J. J. Szente, E. W. Kaiser, J. Shi, J. Phys. Chem. 98 (1994) 2083-2089.

[6] T. P. W. Jungkamp, A. Kukui, R. N. Schindler, Ber. Bunsen-Ges. Phys. Chem. 99 (1995) 1057-1066.

[7] P. Biggs, C. E. Canosa-Mas, J. M. Fracheboud, D. E. Shallcross, R. P. Wayne, Geophys. Res. Lett. 22 (1995) 1221-1224.

[8] V. Daele, G. Poulet, J. Chim. Phys. 93 (1996) 1081-1099.

[9] P. Biggs, C. E. Canosa-Mas, D. E. Shallcross, A. Vipond, R. P. Wayne, J. Chem. Soc., Faraday Trans. 93 (1997) 2701-2705.

[10] B. Du, W. Zhang, Chem. Phys. 327 (2006) 10-14.

[11] J. Thiebaud, C. Fittschen, Appl. Phys. B: Lasers and Optics 85 (2006) 383-389.

[12] A. Parker, C. Jain, C. Schoemaecker, P. Szriftgiser, O. Votava, C. Fittschen, Appl. Phys. B: Lasers and Optics 103 (2011) 725-733.

[13] O. Votava, M. Masat, A. E. Parker, C. Jain, C. Fittschen, Rev. Sci. Instrum. 83 (2012) 043110.

[14] A. Parker, C. Jain, C. Schoemaecker, C. Fittschen, React. Kinet. Catal. Lett. 96 (2009) 291-297.

[15] E. Farago, B. Viskolcz, C. Schoemaecker, C. Fittschen, J. Phys. Chem. A 117 (2013) 12802-12811.

[16] G. L. Vaghjiani, A. R. Ravishankara, J. Chem. Phys. 92 (1990) 996-1003.

[17] J. Thiebaud, A. Aluculesei, C. Fittschen, J. Chem. Phys. 126 (2007) 186101.

[18] C. Jain, P. Morajkar, C. Schoemaecker, B. Viskolcz, C. Fittschen, J. Phys. Chem. A 115 (2011) 10720-10728.

[19] D. Holscher, C. Fockenberg, R. Zellner, Ber. Bunsen-Ges. Phys. Chem. 102 (1998) 716-722.

[20] M. K. Gilles, A. A. Turnipseed, R. K. Talukdar, Y. Rudich, P. W. Villalta, L. G. Huey, J. B. Burkholder, A. R. Ravishankara, J. Phys. Chem. 100 (1996) 14005-14015.

[21] M. A. Teruel, T. J. Dillon, A. Horowitz, J. N. Crowley, Phys. Chem. Chem. Phys. 6 (2004) 2172-2178.

[22] E. A. Selzer, K. D. Bayes, J. Phys. Chem. 87 (1983) 392-394.

[23] R. X. Fernandes, K. Luther, J. Troe, J. Phys. Chem. A 110 (2006) 4442-4449.

[24] R. Atkinson, D. L. Baulch, R. A. Cox, J. N. Crowley, R. F. Hampson, R. G. Hynes, M. E. Jenkin, M. J. Rossi, J. Troe, Atmos. Chem. Phys. 6 (2006) 3625-4055.

[25] R. Zellner, D. Hartmann, J. Karthauser, D. Rhasa, G. Weibring, J. Chem. Soc., Faraday Trans. 84 (1988) 549-568.

[26] M. E. Jenkin, R. A. Cox, J. Phys. Chem. 95 (1991) 3229-3237.

[27] T. J. Dillon, M. E. Tucceri, J. N. Crowley, Phys. Chem. Chem. Phys. 8 (2006) 5185-5198.

[28] S. Enami, T. Yamanaka, S. Hashimoto, M. Kawasaki, Y. Nakano, T. Ishiwata, J. Phys. Chem. A (2006).

[29] C. S. E. Bale, C. E. Canosa-Mas, D. E. Shallcross, R. P. Wayne, Phys. Chem. Chem. Phys. 7 (2005) 2164-2172.

[30] T. J. Dillon, M. E. Tucceri, J. N. Crowley, ChemPhysChem 11 (2010) 4011-4018.

[31] J. Thiebaud, S. Crunaire, C. Fittschen, J. Phys. Chem. A 111 (2007) 6959-6966.

[32] Y. Tang, G. S. Tyndall, J. J. Orlando, J. Phys. Chem. A 114 (2010) 369-378.

[33] M. B. Pushkarsky, S. J. Zalyubovsky, T. A. Miller, J. Chem. Phys. 112. (2000) 10695-10698.

[34] D. B. Atkinson, J. L. Spillman, J. Phys. Chem. A 106 (2002) 8891-8902.

[35] R. Atkinson, D. L. Baulch, R. A. Cox, J. N. Crowley, R. F. Hampson, R. G. Hynes, M. E. Jenkin, M. J. Rossi, J. Troe, Atmos. Chem. Phys. 4 (2004) 1461-1738.

[36] M. Keiffer, A. J. Miscampbell, M. J. Pilling, J. Chem. Soc., Faraday Trans. 84 (1988) 505-514.

[37] C. Fittschen, B. Delcroix, N. Gomez, P. Devolder, J. Chim. Phys. 95 (1998) 2129-2142.

[38] D. L. Baulch, C. J. Cobos, R. A. Cox, P. Frank, G. Hayman, T. Just, J. A. Kerr, T. Murrells, M. J. Pilling, J. Troe, R. W. Walker, J. Warnatz, J. Phys. Chem. Ref. Data 23 (1994) 847-1033.

[39] R. Atkinson, D. L. Baulch, R. A. Cox, J. N. Crowley, R. F. Hampson, R. G. Hynes, M. E. Jenkin, M. J. Rossi, J. Troe, Atmos. Chem. Phys. Discuss. 7 (2007) 981-1191.

[40] H. Hippler, R. Rahn, J. Troe, J. Chem. Phys. 93 (1990) 6560-6569.

Legend of Tables and Figures

Table 1: Reaction mechanism used for numerical simulation of CH_3O_2 and OH decays.

Table 2: Results of fitting individual decays of all O_3 experiments to the mechanism such as shown in Table 1. The error on the average value is statistical only (95% confidence interval).

Figure 1: Red and open gray dots (left y-axis): absolute CH_3O_2 concentrations from cw-CRDS measurements; grey dots are raw data from individual ring-down events, red dots are obtained by averaging over a time window of 1 ms. Insert shows CH_3O_2 decay over 100 ms. Blue dots: relative OH concentrations from simultaneous LIF measurements (right y-scale).

Figure 2: Upper panel: CH_3O_2 concentration time profile, insert shows zoom of the shaded area, representing the same time scale than the OH-decay in the lower panel. Lower panel: OH decay, open dots are experimental LIF intensities, normalized to an estimated initial OH concentration of 10^{10} cm^{-3}, the horizontal dashed line in the insert upper panel and in the lower panel indicates 300 µs. The full line presents a model without secondary chemistry, dotted blue line includes I-chemistry (R14) and (R15), dashed red line is the full model.

Figure 3: Simulation showing the impact of the rate constant of (R16) on the CH_3O_2 profile, full grey and dashed grey lines show the concentration profile of the product of (R16).

Figure 4: Rate constants for the title reaction such as obtained from the simulations of the individual experiments to the full model from Table 1 as a function of initial radical concentration. Open symbols are from experiments at 50 Torr with relatively high O_3 and $O(^3P)$ concentrations (upper part of Table 2), red stars are results from experiments at 100 Torr, containing comparably lower O_3 and $O(^3P)$ concentrations (lower part of Table 2).

Table 1: Reaction mechanism used to simulate CH_3O_2 and OH profiles.

Number	Reaction	Rate constant	Ref.
1	$CH_3O_2 + OH \rightarrow$ products	varied	This work
4 a 4 b	$2\ CH_3O_2 \rightarrow 2\ CH_3O + O_2$ $\rightarrow CH_2O + CH_3OH + O_2$	1.3×10^{-13} 2.2×10^{-13}	[24]
5	$CH_3O_2 + HO_2 \rightarrow CH_3O_2H + O_2$	5.2×10^{-12}	[24]
6	$CH_3I + h\nu_{248nm} \rightarrow CH_3 + I$		
7	$CH_3 + O_2 \rightarrow CH_3O_2$	$1.4 / 2.1 \times 10^{-13}$	[22,[23]
10	$OH + O(^3P) \rightarrow O_2 + H$	3.5×10^{-11}	[35]
11	$OH + O_3 \rightarrow HO_2 + O_2$	7.3×10^{-14}	[35]
12 a 12 b 12 c	$O(^3P) + CH_3I \rightarrow CH_3 + OI$ $\rightarrow OH + CH_2I$ $\rightarrow$ products	7.5×10^{-12} 2.7×10^{-12} 7.3×10^{-12}	[20]
13	$O(^3P) + CH_3O_2 \rightarrow CH_3O + O_2$	4.3×10^{-11}	[25]
14	$CH_3O_2 + I \rightarrow CH_3O_2I$	2×10^{-11}	[27]
15	$CH_3O_2\ I + I \rightarrow CH_3O_2 + I_2$	1.5×10^{-10}	[27]
16	$CH_3O_2 + OI \rightarrow$ products	3.4×10^{-12}	[30]
17	$CH_3 + CH_3O_2 \rightarrow 2\ CH_3O$	9.1×10^{-11}	[36]
18	$CH_3O + O_2 \rightarrow CH_2O + HO_2$	1.9×10^{-15}	[24]
19	$CH_3O + CH_2O \rightarrow$ products	2.3×10^{-14}	[37]
20	$2\ HO_2 \rightarrow H_2O_2 + O_2$	1.7×10^{-12}	[35]
21	$2\ CH_3 \rightarrow C_2H_6$	6×10^{-11}	[38]
22	$OH + I_2 \rightarrow IOH + I$	2.1×10^{-10}	[39]
23	$O(^3P) + O_3 \rightarrow 2\ O_2$	8×10^{-15}	[35]
24	$O(^3P) + O_2\ (+M) \rightarrow O_3\ (+M)$	3.36×10^{-34}	[40]

Table 2: Results of fitting individual decays of all O_3 experiments to the mechanism such as shown in Table 1. The error on the average value is statistical only (95% confidence interval).

CH_3I / 10^{14} cm^{-3}	E / mJ cm^{-2}	$[CH_3]_0 = [I]_0$ / 10^{12} cm^{-3}	k_1 / 10^{-10} cm^3 s^{-1}
p = 50 Torr. $[O_2] = 5\times10^{17}$ cm^{-3}, $[O_3] \approx 1.5\times10^{13}$ cm^{-3}, $O(^3P) \approx 5\times10^{12}$ cm^{-3}			
7.9	21	18.0	3.0
4.9	21	14.0	2.8
3.1	21	8.4	2.8
1.8	21	4.3	2.8
6.7	13.4	13.5	2.6
5.3	13.4	10.4	2.6
3.1	13.4	5.4	2.6
1.8	13.4	3.0	2.6
4.9	13.4	9.4	2.75
p = 100 Torr, $[O_2] = 1.9\times10^{17}$ cm^{-3}, $[O_3] \approx 0.3\times10^{13}$ cm^{-3}, $O(^3P) \approx 1\times10^{12}$ cm^{-3}			
6.6	13.4	10.5	3.0
5.4	13.4	7.9	3.2
4.2	13.4	6.4	2.8
3.0	13.4	4.4	2.9
1.7	13.4	2.2	3.3
1.7	20	3.6	2.95
1.7	22	4.5	2.6
3.0	22	7.2	2.8
3.0	18	6.6	2.8
4.2	18	8.8	2.75
4.2	22	10.2	2.85
5.4	22	13.6	2.6
5.4	18	11.0	2.8
6.6	18	13.7	2.5
6.6	22	16.4	2.8
		Average:	$(2.80 \pm 0.06) \times 10^{-10}$

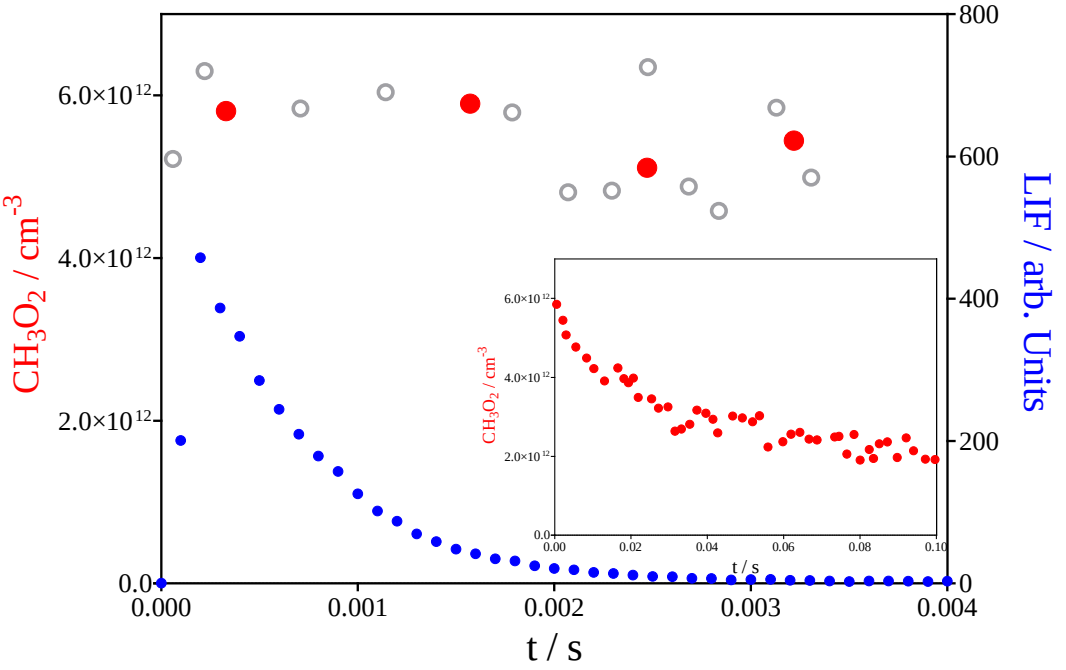

Figure 1: Red and open gray dots (left y-axis): absolute CH_3O_2 concentrations from cw-CRDS measurements; grey dots are raw data from individual ring-down events, red dots are obtained by averaging over a time window of 1 ms. Insert shows CH_3O_2 decay over 100 ms. Blue dots: relative OH concentrations from simultaneous LIF measurements (right y-scale).

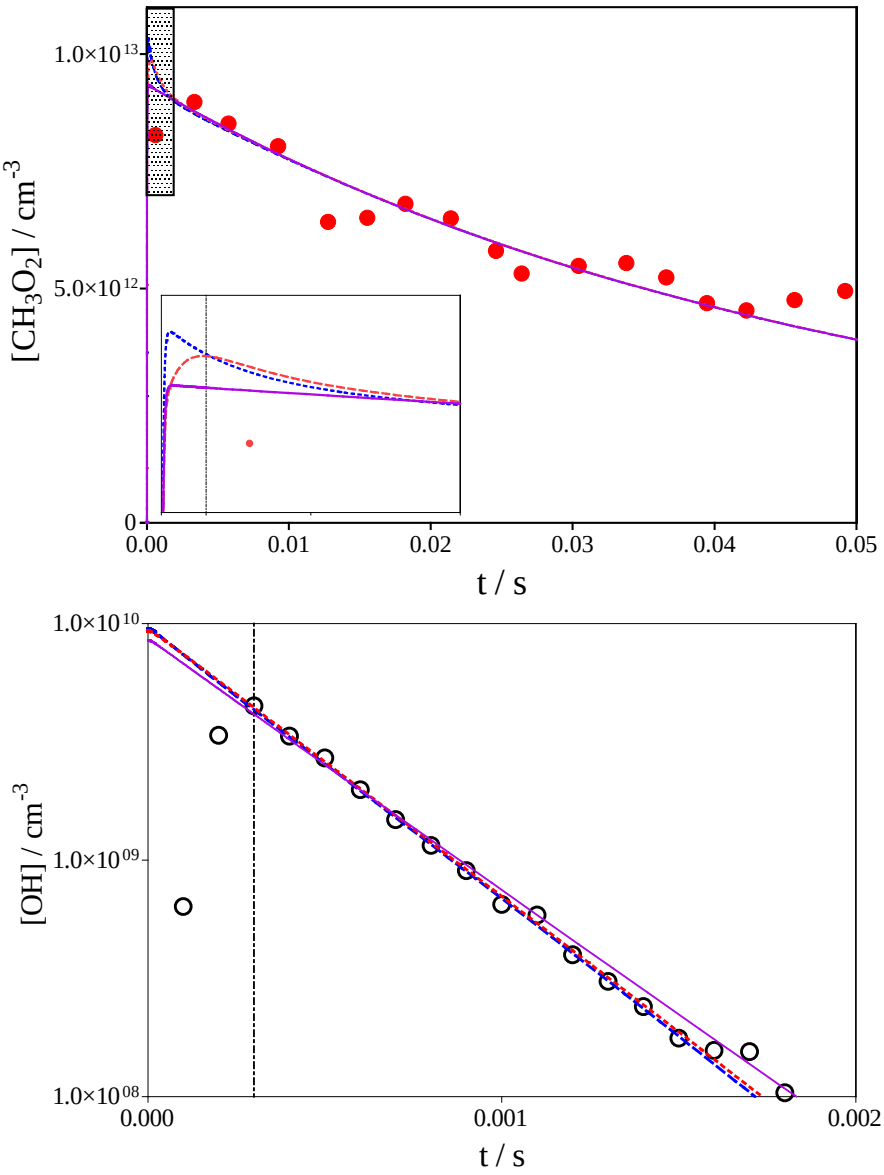

Figure 2: Upper panel: CH_3O_2 concentration time profile, insert shows zoom of the shaded area, representing the same time scale than the OH-decay in the lower panel. Lower panel: OH decay, open dots are experimental LIF intensities, normalized to an estimated initial OH concentration of 10^{10} cm^{-3}, the horizontal dashed line in the insert upper panel and in the lower panel indicates 300 µs. The full line presents a model without secondary chemistry, dotted blue line includes I-chemistry (R14) and (R15), dashed red line is the full model.

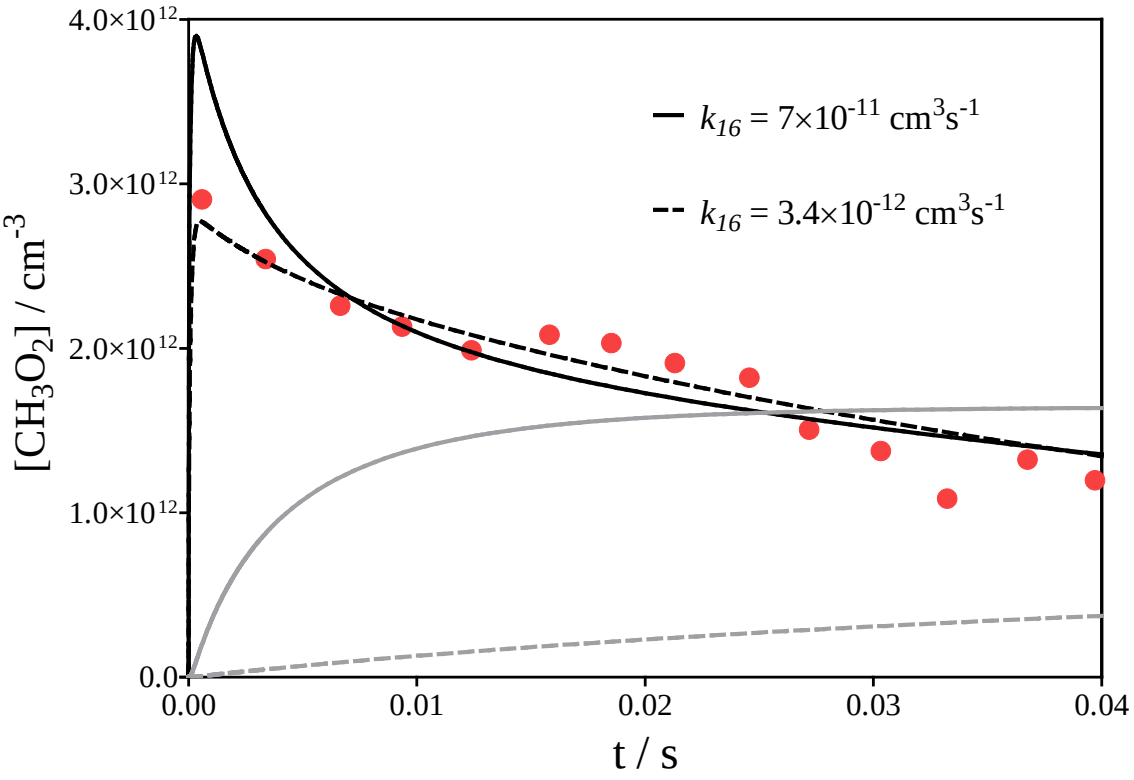

Figure 3: Simulation showing the impact of the rate constant of (R16) on the CH_3O_2 profile, full grey and dashed grey lines show the concentration profile of the product of (R16).

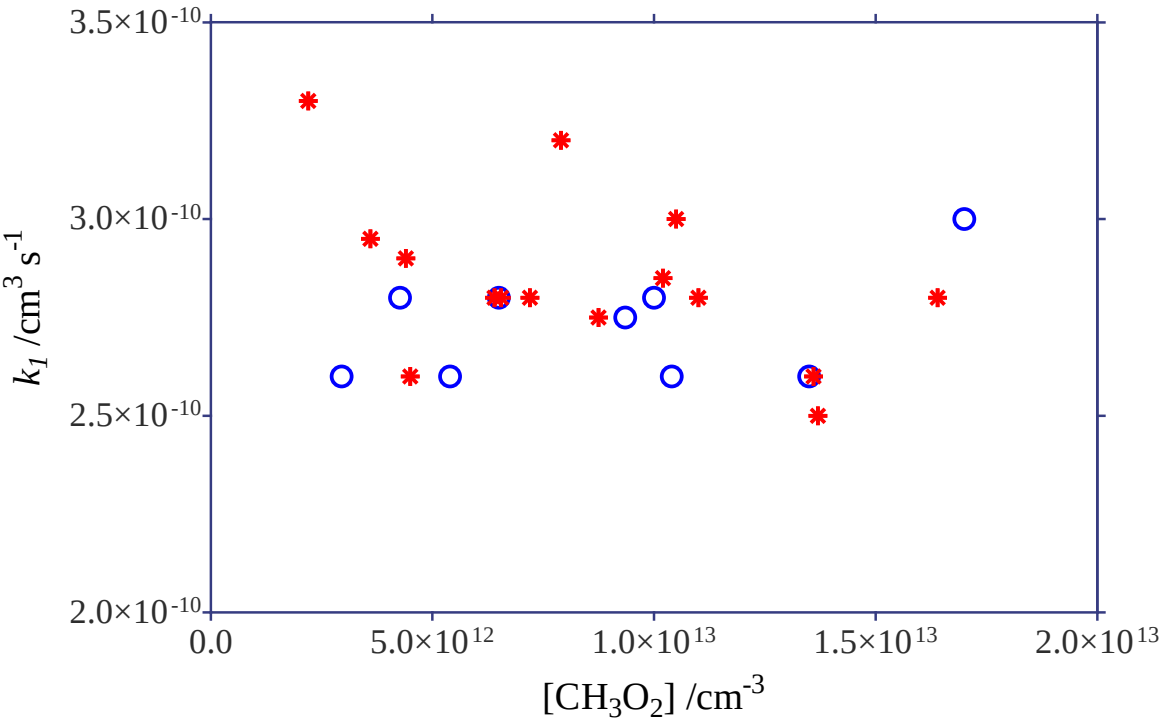

Figure 4: Rate constants for the title reaction such as obtained from the simulations of the individual experiments to the full model from Table 1 as a function of initial radical concentration. Open symbols are from experiments at 50 Torr with relatively high O_3 and $O(^3P)$ concentrations (upper part of Table 2), red stars are results from experiments at 100 Torr, containing comparably lower O_3 and $O(^3P)$ concentrations (lower part of Table 2),